Effects of piezo-spectroscopic coefficients of 8 wt.% Y_2O_3 stabilized ZrO_2 on residual stress measurement of thermal barrier coatings by Raman spectroscopy

W. G. Mao [(a,b)*], Q. Chen [(a,b)], C. Y. Dai [(a,b)], L. Yang[(a,c)], Y. C. Zhou[(a,b)], C. Lu[(d)]

[(a)] Faculty of Materials, Optoelectronics and Physics, Xiangtan University, Hunan 411105, China

[(b)] Key Laboratory of Low Dimensional Materials & Application Technology, Ministry of Education, Xiangtan University, Hunan 411105, China

[(c)] State Key Laboratory of Explosion Science and Technology, Beijing Institute of Technology, Beijing 100081, China

[(d)] Department of Mechanical Engineering, Curtin University of Technology, Perth, Western Australia 6845, Australia

Abstract

By using specially designed freestanding 8 wt.% Y_2O_3 stabilized ZrO_2 (8YSZ) specimens, a linear relationship is found between the Raman peak shift, $\Delta\omega$, and applied uniaxial compressive stress, $\bar{\sigma}_u$, i.e., $\Delta\omega = \Pi_u \cdot \bar{\sigma}_u$ with Π_u being the piezo-spectroscopic coefficient. The linear relationship is used to determine the in-plane residual stress in air plasma sprayed 8YSZ thermal barrier coatings (TBCs). It is shown that the Π_u of the 8YSZ is an exponential function of the thermal cycle N for a given thermal cycling process: $\Pi_u = 37.6\exp(-N/25.9)+13$. Based on these two relationships, the actual residual stress of 8YSZ TBCs determined by the Raman spectroscopy method is quantitatively consistent with that obtained by the X-ray diffraction.

Keywords: thermal barrier coating; piezo-spectroscopic coefficient; Raman spectroscopy; residual stress

* Corresponding author: W. G. Mao, Faculty of Materials, Optoelectronics and Physics, Xiangtan University, Hunan 411105, China. E-mail: ssamao@xtu.edu.cn , Tel.: +86-731-58298580, Fax: +86-731-58292468.

1. Introduction

Thermal barrier coatings (TBCs) composed of NiCrAlY bond layers and 8 wt.% Y_2O_3-stabilized ZrO_2 (8YSZ) ceramic top layers have been widely applied in stationary turbines of power plants and aircraft turbines in order to protect basic materials (e.g., advanced Ni-superalloys) from high temperature and corrosion, and thereby increase their component lives [1-3]. However, the residual stress in TBCs gradually accumulates during the long-term application due to the mismatch of material properties and high-temperature oxidation, which may directly cause adhesive failure (delamination at interface) or cohesive failure (spalling or microcracking within ceramic coating) [3-7]. Early studies showed that, for electron beam physical vapor deposited TBCs, fracture mainly locates between the thermally grown oxide (TGO) and top coat interface, and for air plasma-sprayed (APS) TBCs, failure mostly occurs within the top coat close to the coating and TGO interface [1, 2]. Therefore, residual stress plays an important role in predicting the performance and lifetime of the TBCs [8, 9]. Several engineering methods have been developed to evaluate the evolution of residual stress in various kinds of TBCs, such as X-ray diffraction (XRD), neutron diffraction, substrate removal, Raman spectroscopy [10-15], curvature measurement and photo-stimulated luminescence piezospectroscopy (PLPS) [16-19]. It is noteworthy that the PLPS technique can be used for measuring residual stress in the TGO and determining the type of TGO (such as α, θ, γ alumina). The PLPS also has the potential to provide the accurate quality control, nondestructive inspection, remaining life assessment, and lifetime prediction for TBCs [19-21]. But the PLPS can't be easily applied to measure residual stresses in the top coat due to the lack of chromium (Cr^{3+}). So the stress distribution in the top coat is usually determined by Raman spectroscopy based on the measurement of the Raman piezo-spectroscopic coefficient (PSC) [11, 14, 15, 22, 23]. The Raman peak shift is connected with temperature and pressure [24, 25]. Teixeira *et*

al. obtained a linear relationship between applied stress and Raman peak shift in the zirconia coatings with the PSC of approximately 220 cm^{-1}/MPa [11]. Cai *et al.* investigated the stress-induced frequency shifts of the Raman band in as-received YSZ and found that the PSC increases with the concentration of Y_2O_3 [14]. Such a linear relationship has also been found by Tanaka *et al*. for the stress-Raman frequency shift of an extracted freestanding as-received 8YSZ layer under uniaxial compressive tests, and the PSC is about 25 cm^{-1}/GPa [15]. Limarga *et al*. reported the PSCs of all the Raman bands of the 7YSZ material under uniaxial compressive stress [16]. However, to the best of our knowledge, there are still no reports on the evolution of PSCs with thermal cycles of 8YSZ, which would be helpful to measure the evolution of residual stress in 8YSZ TBCs by Raman spectroscopy in service. The goal of the paper is to measure the PSCs evolution of 8YSZ with thermal cycles by stress-Raman frequency shift method. The effects of Young's modulus and thermal cycling on the evolution of PSCs were considered and discussed. The evolution of residual stress in 8YSZ TBCs specimens was evaluated using the stress-Raman shift relationship with varied PSCs.

2. Experimental procedure

2.1 Specimen preparation

Two kinds of specimens, a freestanding 8YSZ coating and 8YSZ TBCs specimens, are prepared by the APS technique. The freestanding 8YSZ specimen is used to measure the compressive stress-Raman frequency shift relationship. The related preparation process is as follows, stainless steel with a volume of 150×50×10 mm^3 is selected as substrate and a few rectangle grooves with 50×5×5 mm^3 are cut crosswise. Then, the 8YSZ powder is deposited into these rectangle grooves. The coated stainless steel substrate is carefully incised and slowly grinded by the commercial

cutting machine (IsoMet® 4000) and grinding miller (Beta™). The extracted 8YSZ bar is obtained after the stainless steel is removed. These bars are cut again and polished to form rectangular shape freestanding specimens with 15×4.5×2.5 mm^3. The specimen surface is finely polished with 2.5 μm diamond paste. All the freestanding 8YSZ specimens are carefully cleaned by ultrasonic oscillator and completely blown dry. For APS 8YSZ TBCs specimens, the geometry size is 20×5×2.4 mm^3. The material of substrate, bond coat and coating is Ni-superalloy, NiCrAlY and 8YSZ, respectively. The thickness of substrate, bond coat and 8YSZ coating is 2 mm, 0.1 mm and 0.30 mm, respectively. The detailed APS preparation process is given in the reference [7]. In our work, the total amount of the freestanding 8YSZ and 8YSZ TBCs specimens is 18 and 12, respectively.

2.2 Thermal cycling experiment

To simulate the high-temperature exposure inside a turbine, two kinds of specimens were exposed to thermal cycling in a high temperature furnace. Each thermal cycle consists of a 10-min heat-up from room temperature to 1000 ^{o}C, a 40-min holding at 1000 ^{o}C, and a 10-min forced air quench. For freestanding 8YSZ specimens, thermal cycling is 100, 200, 250, 300, 400, and 500 cycles, respectively. For 8YSZ TBCs specimens, thermal cycling is 50, 100, and 180 cycles, respectively. Three samples were tested for each case. Fig. 1 shows the scanning electron microscope (SEM) micrographs of surface microstructure changes of the freestanding 8YSZ specimens with thermal cycles. The microscope apparatus model is JSM-6360. Fig. 1(a) indicates the original microstructure of as-received specimen. There are a large amount of pores in conjunction with a platelet (or splat) structure. After annealed 200 and 300 thermal cycles, it can be seen that a noticeable sintering phenomenon of the 8YSZ occurs, as shown in Figs. 1(b) and 1(c), which would result in 8YSZ material densification, along with substantial grain growth in some

regions. The changes of microstructure may result in the changes of its thermomechanical and thermophysical properties of the freestanding 8YSZ coating [26, 27].

2.3 In-plane effective Young's modulus

It has been proved that the Young's modulus of the 8YSZ coating is dependent on factors such as porosity level, micro-cracks, thermal aging time, preferred orientation and crystalline structure [28, 29]. To determine the Young's modulus of the freestanding 8YSZ specimens, uniaxial compression tests are performed by a mechanical testing device (the equipment model: REGER 2000-10). Each specimen is loaded to 20 N with a rate of about 0.015 mm/min by displacement control mode. Strain gauges are applied to measure the axial deformation of the tested specimens. It is worth noting that the deformation of the freestanding 8YSZ specimens is limited at the elastic stage. Thus, the in-plane Young's modulus E of the freestanding 8YSZ specimens can be obtained by

$$E = \frac{P}{h \cdot w \cdot \varepsilon} \tag{1}$$

where P is the applied load, ε is the axial compressive strain measured by strain gauge, and h and w are the thickness and width of the specimen, respectively.

2.4 Micro-Raman spectroscopy test

As illustrated in Fig. 2, a freestanding specimen is loaded under uniaxial compression in a stepwise manner by whirling the bolt. A strain gauge is adhered onto the bottom of the specimen surface in order to measure the axial strain. All Raman spectra are taken at room temperature in backscattering mode with a power of 30 mW at the 488 nm line of an Ar^+ laser (HR-600, France). The instrumental resolution of the Raman spectroscope in wave number is 0.65 cm^{-1}, and the

measured wave number range is from 100 to 700 cm^{-1} with the irradiation time at ~30 s per spectrum. The laser beam is focused on the sample, using a 50× objective lens, and the dimension of the laser is ~2 μm. The polarization of the incident beam is parallel to the direction of uniaxial stress. The spectra are taken from the same location near the mid-point of samples and identified by features observed under a microscope. The Raman spectra near the top of the peaks are fitted into the Lorentzians curve to determine the values of peak positions. In tests, specimens are carefully aligned along the load axis to ensure a uniform uniaxial compression. However, the buckling effect of the freestanding 8YSZ specimen under the in-plane compressive state should be avoided. Therefore, the compressive stress is controlled and made much lower than the estimated stress of buckling.

2.5 X-ray diffraction

To identify the phase structure of the freestanding 8YSZ, specimens were examined before and after thermal aging by XRD (D/Max 2550) with filtered Cu radiation at 40 KV and 250 mA. The XRD profile of the freestanding 8YSZ specimens with well identified peaks is shown in Fig. 3. It is seen that these specimens mainly consist of tetragonal and cubic phase. And this indicates that the heat treatment has no major influence on the phase structures of the 8YSZ in this work. Furthermore, to confirm the reliability of the results obtained from Raman measurements, XRD was also carried out to evaluate the residual stress distribution of 8YSZ TBCs specimens. For a biaxial stress state, the lattice spacing (or strain) is related to the stress by [11, 30]

$$\frac{d_{\phi\psi}-d_0}{d_0}=\frac{1+\nu}{E}\sigma_\phi \sin^2\psi-\frac{\nu}{E}\left(\sigma_{11}+\sigma_{22}\right) \tag{2}$$

where d_0 and $d_{\phi\psi}$ are the unstressed and stressed lattice spaces, respectively, σ_ϕ is the stress

component along the direction ϕ. ψ is the tilt angle. σ_{11} and σ_{22} are stress components along the principal directions, respectively. It is obvious that there is a linear relationship between $d_{\phi\psi}$ and $\sin^2\psi$. The stress can be obtained by a least-square-fit of experimentally determined *d*-spacing at a number of ψ tilts. The reflection used in residual stress analysis was the (312) for 8YSZ at about 95°. The diffraction angle 2θ ranged from 93.5° to 96.5° in steps of 0.02°.

3. Results and discussion

3.1 Evolution of Young's modulus

As shown in Fig. 4, the Young's modulus E of the freestanding 8YSZ specimen is a function of the thermal cycles *N*. It increases from 10 GPa (as-received specimen) to 32 GPa at 150 thermal cycles. The Young's modulus E retains a constant at about 32 GPa within the subsequent thermal cycles. The experimental data can be fitted by

$$E = 34.4 - 24.4 \times \exp(-N / 71.4) \quad (3)$$

where *N* is the number of thermal cycling. The evolution of Young's modulus exhibits two different stages of stiffening, i.e. an initially rapid rise, followed by a more progressive increase. The similar results were also observed by other researchers [31, 32]. The rapid rise stage is due to the sintering effect (see Fig. 1), which strengthens bonding between splats and blocks sliding along splat boundaries. And the second stage may attribute to the recovery of microcracks [32, 33]. In addition, the freestanding 8YSZ coating is held together mainly by mechanical interlocking between splats. Thus, when the coating is loaded, it deforms in a way that splats slide against each other along splat boundaries in the forced direction. The sliding results in macro-deformation and a low value of Young's modulus E [34].

3.2 Raman spectrum analysis

Figure 5 shows a typical Raman spectrum of the 8YSZ coating in the region of 100 to 700 cm^{-1}, where four well identified peaks are the tetragonal phases of ZrO_2. The peak around 640 cm^{-1} is usually selected for the stress analysis [11, 14]. Here, this characteristic peak is used for the stress-Raman frequency shift measurement of the freestanding 8YSZ specimens in our work. As shown in Fig. 6, a linear relationship is obtained between the Raman frequency shift $\Delta\omega$ and the applied uniaxial compressive stress $\overline{\sigma}_u$ for freestanding 8YSZ specimens. Assumed that the freestanding 8YSZ layer is under a plane stress state [15, 22], we have

$$\Delta\omega = \Pi_u \cdot \overline{\sigma}_u \tag{4}$$

where Π_u is the PSC as mentioned above, which represents the stress sensitivity of Raman band, and $\Delta\omega = \omega_s - \omega_o$ with ω_o being the peak position of the stress-free state and ω_s the peak position of the stressed state. Experimental results indicate that the Raman characteristic peak ω_o is approximately a constant for as-received and annealed freestanding 8YSZ specimens. The PSC values of the different types freestanding 8YSZ specimens can be obtained from the slopes by fitting the $\overline{\sigma}_u$ *and* $\Delta\omega$ experimental data. The data analysis indicates that the PSCs are 50.57, 13.76, 13.85, 9.01, 16.34 and 12.73 cm^{-1}/GPa for as-received and annealed (100, 200, 250, 300 and 400 cycles) freestanding 8YSZ specimens, respectively. It is obvious that the PSCs of the freestanding 8YSZ are significantly influenced by thermal cycling, which can be used in measuring residual stress in the 8YSZ TBCs by Raman spectroscopy method. The evolution of the PSCs with thermal cycles can be fitted by the following formula for a given thermal cycling, as shown in Fig. 7,

$$\Pi_u = 37.6\exp(-N/25.9) + 13 \tag{5}$$

It is worth noting that, however, Eq. (5) is only valid for the peak around 640 cm^{-1} of the APS

8YSZ. Given an applied stress, $\bar{\sigma}_u$, the PSC Π_u is proportional to the measured Raman shift ω_s and the stress-induced Raman shift ω_s is inversely proportional to Young's modulus of the freestanding 8YSZ coating [35]. Thus, the variation of the PSCs is opposite to the evolution of Young's modulus with thermal cycles. So the variation of the PSCs follows an exponential decay with thermal cycles, which may be due to the increase of Young's modulus with thermal cycles. In previous studies, the PSC was measured only for as-received APS YSZ specimens [14, 15]. Although the PSCs of as-received freestanding 8YSZ are varied, they are still in the same order of magnitudes. Therefore, it is believed that the accuracy of measurement of residual stress may be improved if the evolution of PSCs of the APS 8YSZ is taken into account during Raman spectroscopy tests. The validity of the above results will be proved by measuring residual stress in 8YSZ TBCs specimens by Raman spectroscopy method and XRD.

3.3 Measurement of residual stress for 8YSZ TBCs

For simplification, the in-plane surface residual stress in the top coat of 8YSZ TBCs specimens before and after heat treatment is assumed to be in bi-axial plane stress state (i.e., $\bar{\sigma}_{xx} = \bar{\sigma}_{yy}$, $\bar{\sigma}_{zz} = 0$). The relationship between the residual stress and Raman peak frequency shift can be rewritten as [15],

$$\bar{\sigma}_{xx} = \bar{\sigma}_{yy} = \frac{\Delta\omega}{2\Pi_u} \tag{6}$$

where the Π_u can be obtained by Eq. (5). So the residual stress in the top coat of 8YSZ TBCs can be evaluated by Eq. (6) after the Raman shifts, $\Delta\omega$, of each specimen are determined.

Table 1 shows the residual stress in the surface region of 8YSZ TBCs tested by Raman spectroscopy method and XRD. Considering the evolution of PSCs, the values of residual stress measured by Raman spectroscopy method changed from −11 MPa to −220 MPa with thermal cycles.

And the values of residual stress obtained by XRD increased from −82 MPa to −190 MPa with thermal cycles. Teixeira *et al*. [11] measured the residual stress in the top coat of 8YSZ TBCs after thermal cycling by XRD, which varied from −100 MPa to −250 MPa. The compressive residual stress arises in the coating during thermal cycling owing to the mismatch of thermal expansion coefficient between the 8YSZ and substrate. The residual stress increases rapidly at the beginning stage of the thermal cycling, and it increases tardily after 100 thermal cycles. This evolution of residual stress may be influenced by the following crucial factors, mismatch of materials properties, elastic-plastic deformation, high-temperature creep, interface oxide, coating sintering and so on [36, 37, 38]. The results are similar to the previous investigations [37, 38]. For as-received 8YSZ TBCs specimen, there are a few discrepancies in the measurement results by Raman spectroscopy and XRD. By analyzing the Raman spectra, we find the reason may be that the Raman peak around 640 cm^{-1} of the as-received 8YSZ TBCs specimen is broader than other annealed specimens, which make it difficult to accurately measure the Raman shift of the as-received specimens. But we found that the change trend and magnitude order of the tested residual stress by Raman spectroscopy consist well with that by XRD, except for as-received 8YSZ TBCs situation. So the validity of the evolution of PSCs has been proved by comparing measurement results between Raman spectroscopy and XRD. It means that the evolution of the PSCs of 8YSZ with thermal cycles should be taken into consideration while applying Raman spectroscopy method. In this work, we mainly measured residual stress near the surface region of 8YSZ TBCs specimens due to the limitation of the penetration depth of Raman spectroscopy and XRD technique. And these stresses have little to do with the damage initiation and progression occurring at the TGO/YSZ interface.

4. Conclusions

In this paper, we have studied the stress-Raman frequency shift relationship of the freestanding APS 8YSZ before and after heated treatment. The results show that there is a linear relationship between the applied uniaxial compressive stress of an extracted freestanding 8YSZ coating and Raman frequency shift. The variation of the PSCs in 8YSZ follows an exponential decay with thermal cycles. The functionality and reliability of coated devices are strongly related to the variation of distributions of thermal residual stress. The evolution of the PSCs plays an important role in improving the measurement accuracy of local residual stress of 8YSZ TBCs by Raman spectroscopy method.

Acknowledgments

This work has been supported by the Hunan Provincial Natural Science Foundation (No. 08JJ3003), the Start-up Fund of Xiangtan University (No. 08QDZ07), the Fund for Young Scholars in Hunan Province (No. 08B084), the Young Teacher Fund of Ministry of Education (No. 200805301023), the National Natural Science Foundation of China (No. 10828205), and the Open Project of State Key Laboratory of Explosion Science and Technology of China (No. KFJJ07-7).

References

[1] N.P. Padture, M. Gell, E.H. Jordan, Science 296 (2002) 280-284.

[2] A.G. Evans, D.R. Mumm, J.W. Hutchinson, G.H. Meier, F. S. Pettit, Prog. Mater. Sci. 46 (2001) 505-553.

[3] A.G. Evans, M.Y. He, J. W. Hutchinson, Prog. Mater. Sci. 46 (2001) 249-271.

[4] S.R. Choi, J.W. Hutchinson, A.G. Evans, Mech. Mater. 31 (1999) 431-447.

[5] J.W. Hutchinson, A.G. Evans, Surf. Coat. Technol. 149 (2002) 179-184.

[6] J.W. Hutchinsona, M.Y. He, A.G. Evans, J. Mech. Phys. Solids. 48 (2000) 709-734.

[7] W.G. Mao, C.Y. Dai, Y.C. Zhou, Q.X. Liu, Surf. Coat. Technol. 201 (2007) 6217-6227.

[8] A.N. Khan, J. Lu, H. Liao, Surf. Coat. Technol. 168 (2003) 291-299.

[9] C.H. Hsueh, J. Appl. Phys. 91 (2002) 9652-9656.

[10] D.R. Haeffner, J.D. Almer, U. Lienert, Mater. Sci. Eng. A 399 (2005) 120-127.

[11] V. Teixeira, M. Andritschky, W. Fischer, H.P. Buchkremer, D. Stöver, J. Mater. Process. Technol. 92-93 (1999) 209-216.

[12] N.R. Shankar, H. Herman, S.P. Singhal, C.C. Berndt, Thin Solid Films 119 (1984) 159-171.

[13] C.R.C. Lima, J. Nin, J.M. Guilemany, Surf. Coat. Technol. 200 (2006) 5963-5972.

[14] J. Cai, Y.S. Raptis, E. Anastassakis, Appl. Phys. Lett. 62 (1993) 2781-2783.

[15] M. Tanaka, M. Hasegawa, Mater. Sci. Eng. A 419 (2006) 262-268.

[16] A.M. Limarga, D.R. Clarke, J. Am. Ceram. Soc. 90 (2007) 1272-1275.

[17] X. Zhao, P. Xiao, Surf. Coat. Technol. 201 (2006) 1124-1131.

[18] X. Wang, G. Lee, A. Atkinson. Acta Mater. 57 (2009) 182-195.

[19] M. Wen, E.H. Jordan, M. Gell, Mater. Sci. Eng. A 398 (2005) 99–107.

[20] M. Wen, E.H. Jordan, M. Gell, J. Eng. Gas Turb. Power 128 (2006) 610-616.

[21] M. Gell, S. Sridharan, M. Wen, E.H. Jordan, Int. J. Appl. Ceram. Technol. 1 (2004) 316-329.

[22] L.A. Starman, J.A. Lotta, M.S. Amer, W.D. Cowan, J.D. Busbee, Sensor Actuat. A 104 (2003) 107-116.

[23] H. Miyagawa, D. Kamiya, C. Sato, K. Ikegami, J. Mater. Sci. 34 (1999) 105-110.

[24] P. Bouvier, G. Lucazeau, J. Phys. Chem. Solids 61 (2000) 569-578.

[25] V. Lughi, D.R. Clarke, J. Appl. Phys. 101 (2007) 053524-1.

[26] D.M. Zhu, R.A. Miller, Surf. Coat. Technol. 108 (1998) 114-120.

[27] S. Paul, A. Cipitria, S.A. Tsipas, T.W. Clyne, Surf. Coat. Technol. 203 (2009) 1069-1074.

[28] B. Siebert, C. Funke, R. Vaβen, D. Stöver, J. Mater. Process. Technol. 92 (1999) 217-223.

[29] M. Eskner, R. Sandström, Surf. Coat. Technol. 177 (2004) 165-171.

[30] I.C. Noyan, J.B. Cohen, Residual Stress: Measurement by Diffraction and Interpretation, Springer, Berlin, 1987.

[31] S.Q. Guo, Y. Kagawa, Scripta Mater. 50 (2004) 1401-1406.

[32] J.A. Thompson, T.W. Clyne, Acta Mater. 49 (2001) 1565-1575.

[33] K.F. Wesling, D.F. Socie, J. Am. Ceram. Soc. 77 (1994) 1863-1868.

[34] F. Tang, J.M. Schoenung, Scripta Mater. 54 (2006) 1587-1592.

[35] R.J. Young, Encyc, Mater. Sci. Technol. (2008) 8170-8172.

[36] D.M. Zhu, A.M. Robert, J. Mater. Res. 14 (1999) 146–161.

[37] D.W. Jordan, K.T. Faber, Thin Solid Films 235 (1993) 137-141.

[38] R. Hamacha, B. Dionnet, A. Grimaud, F. Nardou, Surf. Coat. Technol. 80 (1996) 295-303.

Figure captions

Fig. 1. The SEM micrographs of freestanding 8YSZ specimens before and after thermal cycling of (a) as-received, (b) 200, and (c) 300 thermal cycles at 1000°C.

Fig. 2. Schematic of the experimental setup for Raman scattering measurement.

Fig. 3. The X-ray diffraction pattern of freestanding APS 8YSZ before and after thermal cycling.

Fig. 4. Evolution of Young's modulus of the freestanding 8YSZ with thermal cycles.

Fig. 5. Typical Raman spectrum of the as-received freestanding 8YSZ.

Fig. 6. Raman peak frequency shift *versus* applied uniaxial compressive stress in freestanding 8YSZ specimens of (a) as-received and (b) after 400 thermal cycles, where the slopes indicate the PSCs of 8YSZ before and after thermal cycling.

Fig. 7. The PSC of freestanding 8YSZ coating *versus* the thermal cycle.

Table 1

The residual stress in 8YSZ TBCs measured by XRD and Raman spectroscopy.

Thermal cycles, N	σ_{ϕ}, (MPa) [XRD]	$\overline{\sigma}_{xx}$, (MPa) [Raman spectroscopy]
0	- 82	- 11
50	- 138	- 124
100	- 168	- 155
180	- 190	- 220

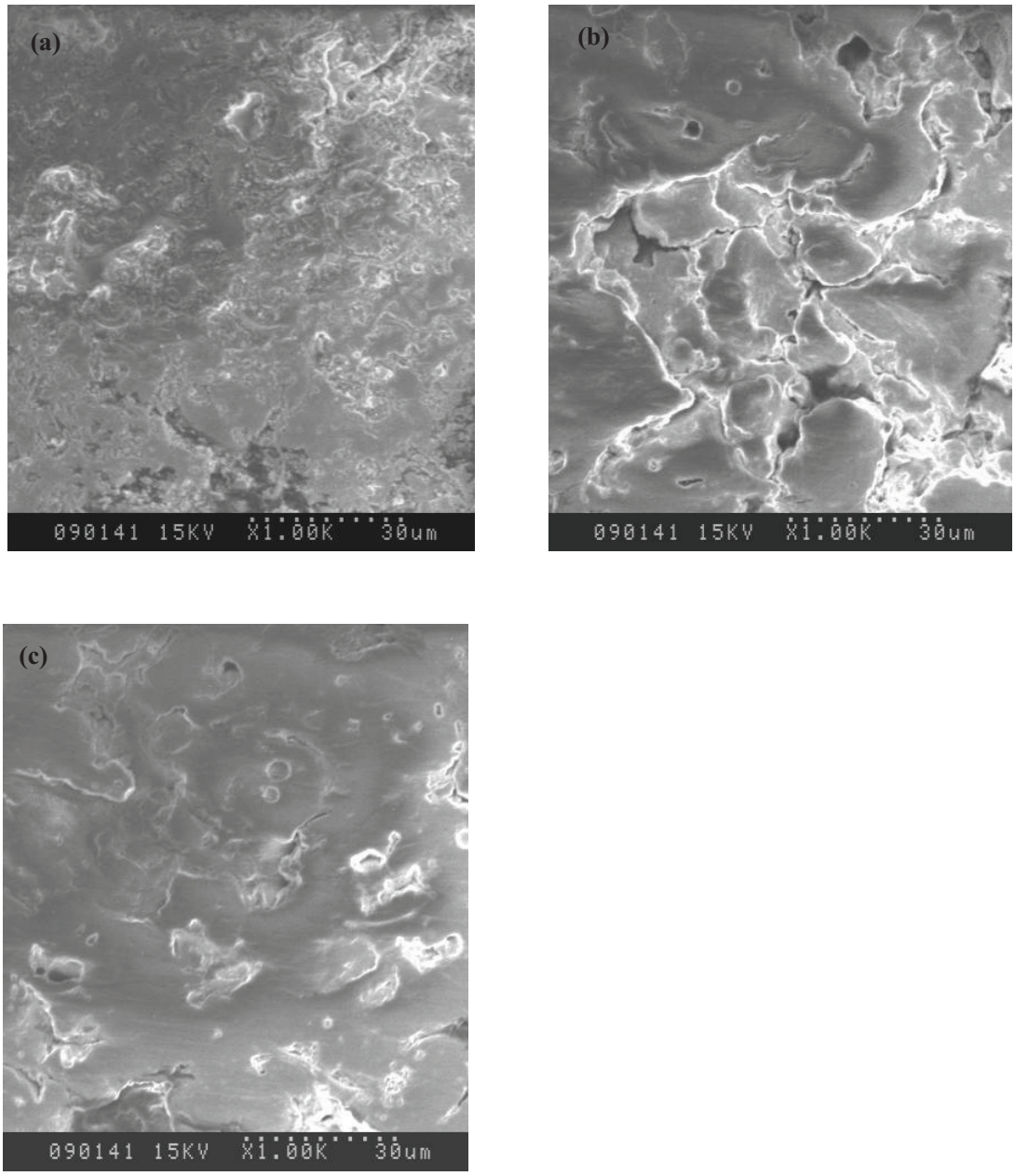
(a)
090141 15KV X1.00K 30um
(b)
090141 15KV X1.00K 30um
(c)
090141 15KV X1.00K 30um

Fig. 1

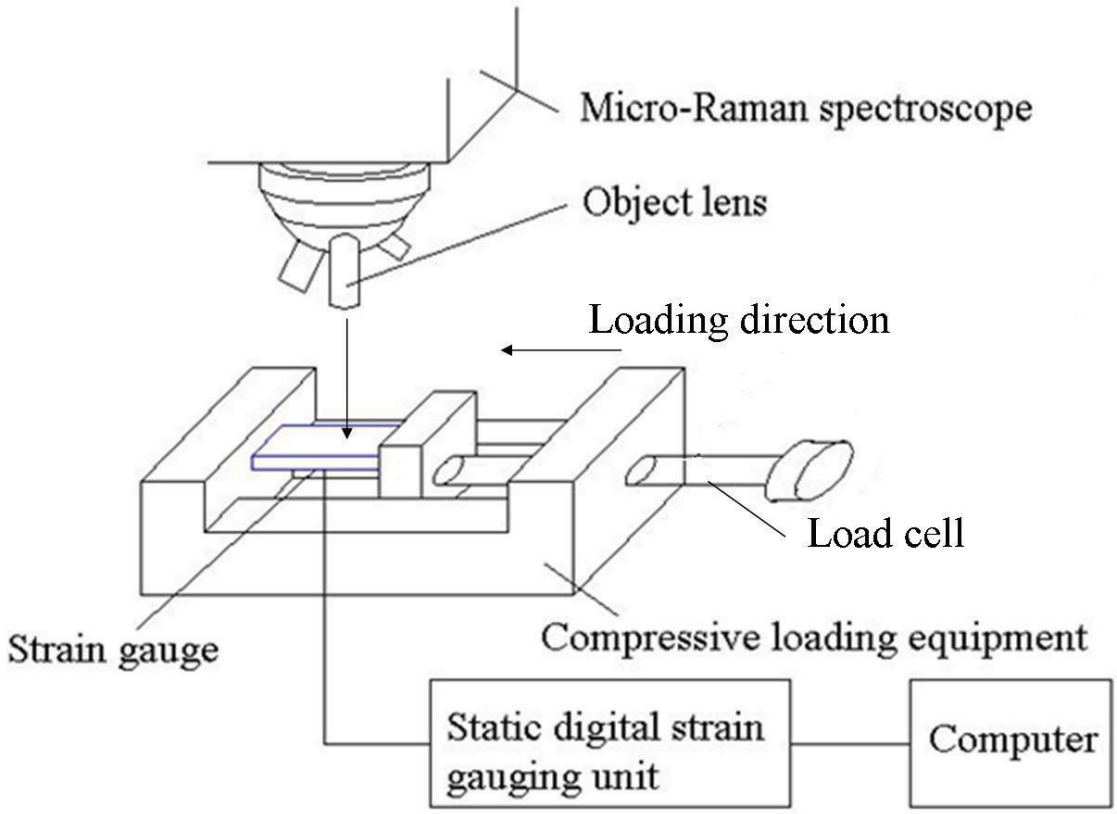
Micro-Raman spectroscope
Object lens
Loading direction
Load cell
Strain gauge
Compressive loading equipment
Static digital strain gauging unit
Computer

Fig. 2

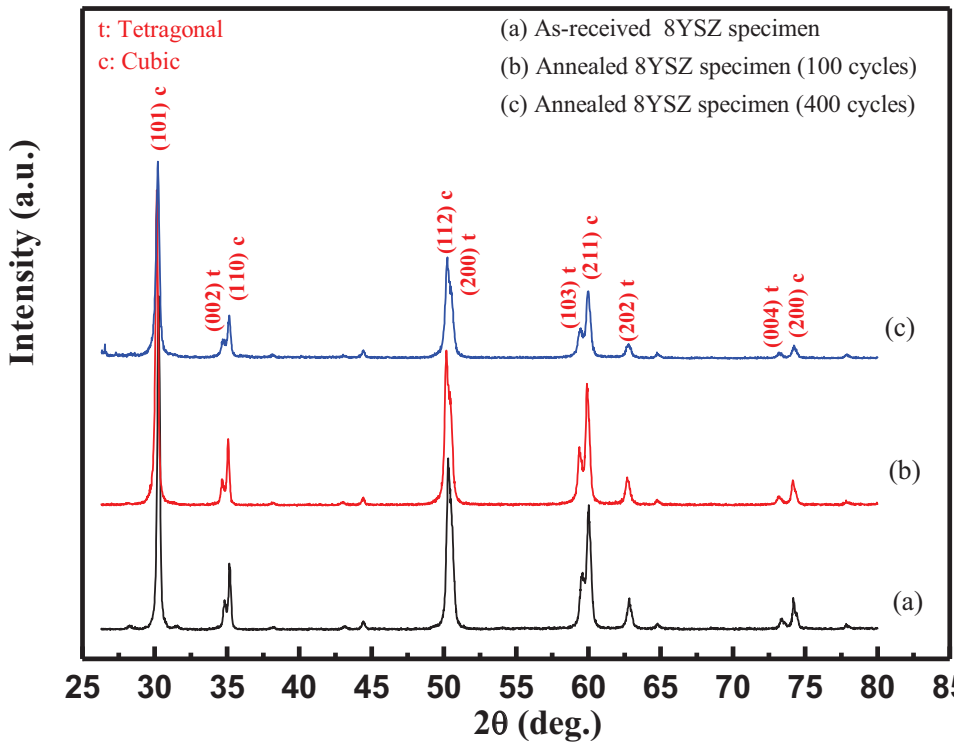
t: Tetragonal
c: Cubic
(a) As-received 8YSZ specimen
(b) Annealed 8YSZ specimen (100 cycles)
(c) Annealed 8YSZ specimen (400 cycles)
(101) c
(002) t
(110) c
(112) c
(200) t
(103) t
(211) c
(202) t
(004) t
(200) c
(c)
(b)
(a)
Intensity (a.u.)
25 30 35 40 45 50 55 60 65 70 75 80
2θ (deg.)

Fig. 3

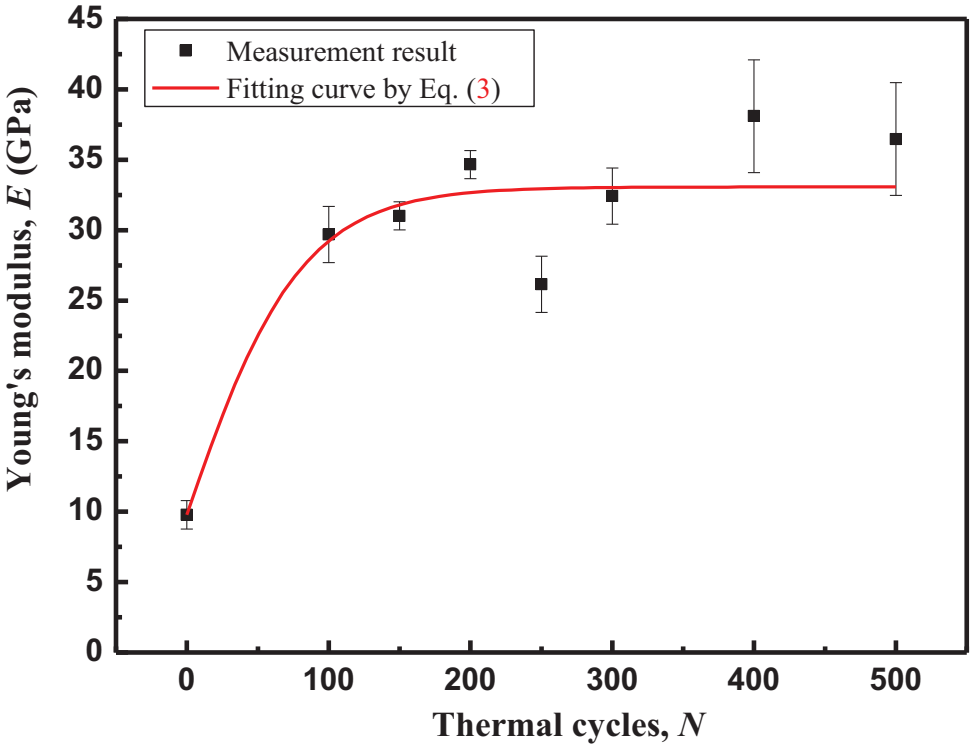
Measurement result
Fitting curve by Eq. (3)
Young's modulus, E (GPa)
Thermal cycles, N
0
5
10
15
20
25
30
35
40
45
0
100
200
300
400
500

Fig. 4

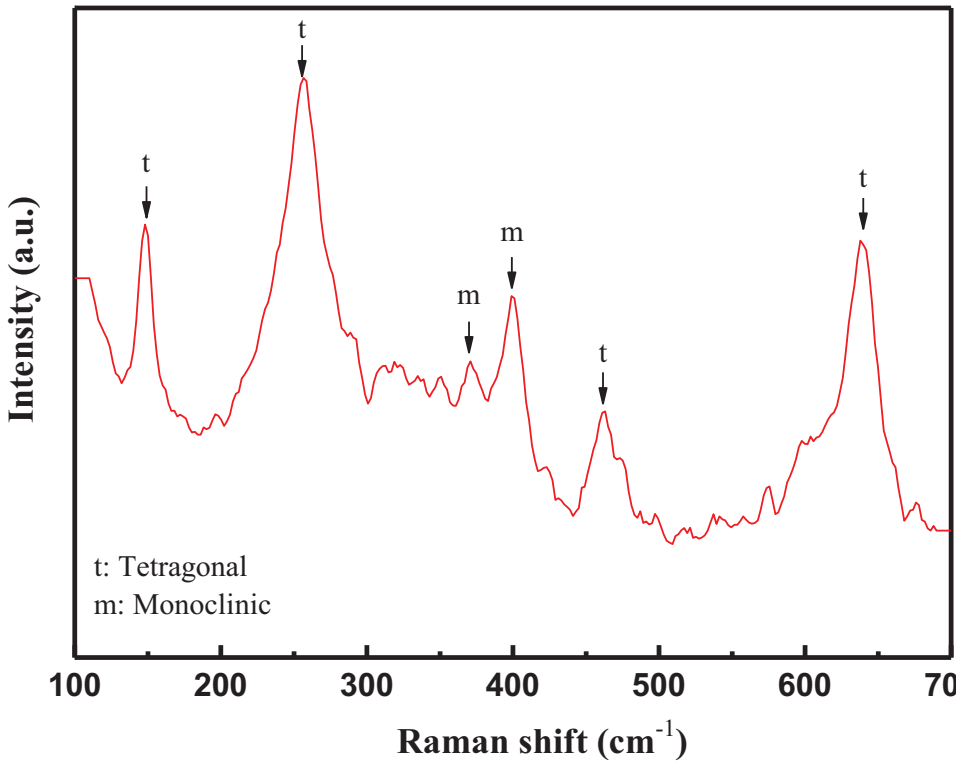
t
t
m
m
t
t
t: Tetragonal
m: Monoclinic
Intensity (a.u.)
100
200
300
400
500
600
70
Raman shift (cm-1)

Fig. 5

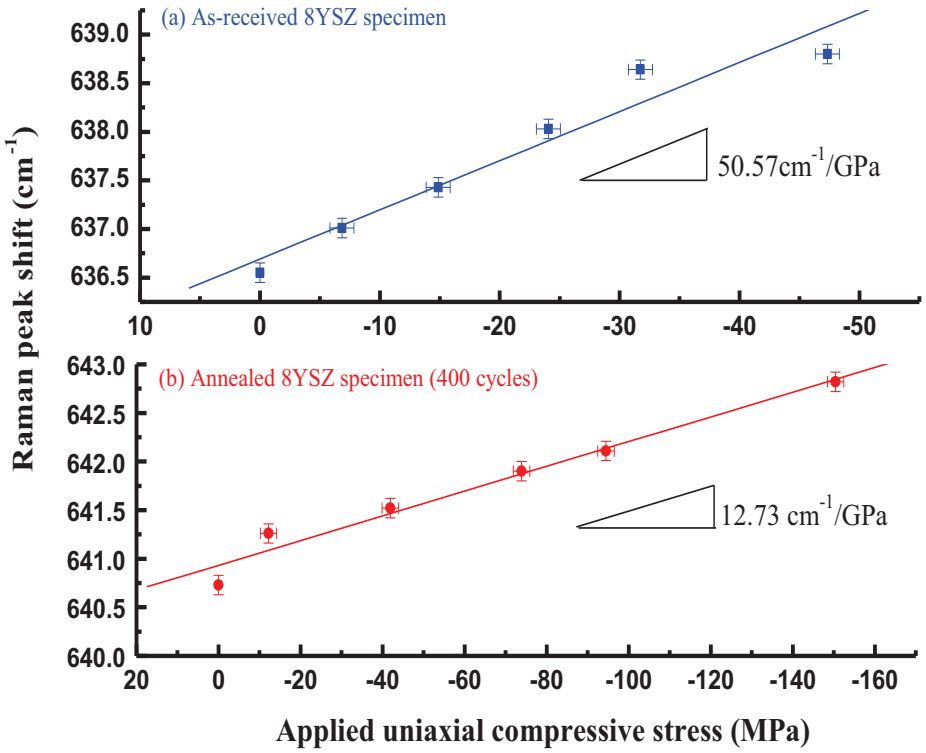
(a) As-received 8YSZ specimen
639.0
638.5
638.0
637.5
637.0
636.5
10
0
-10
-20
-30
-40
-50
50.57cm-1/GPa
(b) Annealed 8YSZ specimen (400 cycles)
643.0
642.5
642.0
641.5
641.0
640.5
640.0
20
0
-20
-40
-60
-80
-100
-120
-140
-160
12.73 cm-1/GPa
Raman peak shift (cm-1)
Applied uniaxial compressive stress (MPa)

Fig. 6

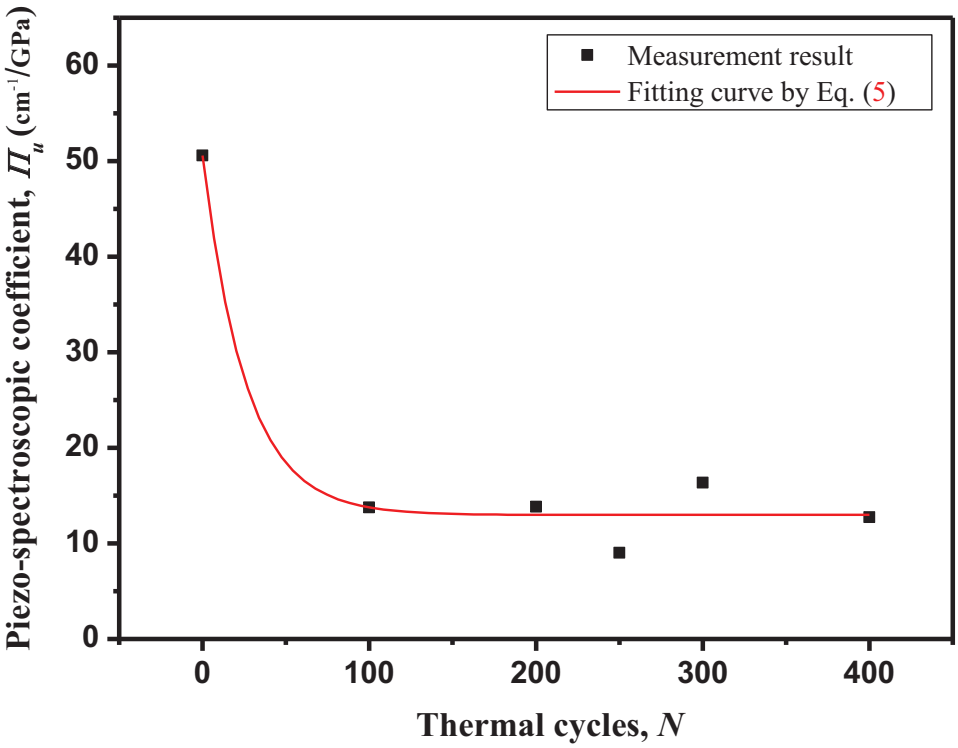
Measurement result
Fitting curve by Eq. (5)
Piezo-spectroscopic coefficient, Π_u (cm^{-1}/GPa)
Thermal cycles, N
0
10
20
30
40
50
60
0
100
200
300
400

Fig. 7